

Quantifying Turbulence for Tidal Power Applications

Jim Thomson
and Brian Polagye

Northwest National Marine Renewable Energy Center
University of Washington,
Seattle, WA 98105
Email: jthomson@apl.washington.edu

Marshall Richmond
and Vibhav Durgesh

Hydrology Group
Pacific Northwest National Laboratory
Richland, WA 99352

Abstract—Using newly collected data from a tidal power site in Puget Sound, WA, metrics for turbulence quantification are assessed and discussed. Of particular interest is the robustness of the “turbulent intensity,” defined as the ratio of velocity standard deviation to velocity mean. Simultaneously, the quality of raw ping Acoustic Doppler Current Profiler (ADCP) data for turbulence studies is evaluated against Acoustic Doppler Velocimeter (ADV) data at a point. Removal of Doppler noise from the raw ping data is shown to be a crucial step in turbulence quantification. Excluding periods of slack tide, the corrected turbulent intensity estimates at a height of 4.6 m above the seabed are 10% and 11% from the ADCP and ADV, respectively. Estimates of the turbulent dissipation rate are more variable, from 10^{-3} to 10^{-1} W/m³. An example analysis of coherent Turbulent Kinetic Energy (TKE) is presented.

I. INTRODUCTION

Advancements in hydrokinetic power generation from tidal currents require detailed understanding of the fluid velocities surrounding devices. Of particular interest are the turbulent fluctuations v' about the mean horizontal velocity $\langle v \rangle$. In the analogous case of wind power generation, these turbulent fluctuations are known to reduce turbine performance and cause material fatigue, which decrease the lifespan of devices. Quantification of turbulence may also be important for assessing environmental effects, because turbulent mixing may contribute to water quality and sediment transport at a given site. The common metric in wind power studies is the turbulence intensity,

$$I = \frac{\sqrt{\langle v'^2 \rangle}}{\langle v \rangle} = \frac{\sigma_v}{\langle v \rangle}, \quad (1)$$

where the brackets indicate an ensemble value using a timescale of statistical stationarity, such that $\sigma_v = \sqrt{\langle v'^2 \rangle}$ is the standard deviation (i.e., the square root of the variance) of the velocity record and $\langle v \rangle$ is the mean (i.e., the expected value). Typical observed values of I are of order 10% at wind power sites. Although convenient, this metric obscures the observed details of the flow, and previous studies have identified the frequency-spectrum of the velocity variance as

a more rigorous quantification of the turbulence [1]. However, it is difficult to obtain high-quality velocity spectra at tidal power sites because of the large standard error in raw ping data from commonly used Acoustic Doppler Current Profilers (ADCPs).

Here, we present new field observations from a proposed tidal power site in Puget Sound, WA (USA) that are used to evaluate the utility of the turbulence intensity metric (Eq. 1) and compare with a more dynamically significant quantity that is related to the spectrum of the velocity variance: the dissipation rate, ϵ , of turbulent kinetic energy, $TKE = \frac{1}{2} \langle v'^2 \rangle$. The dissipation rate is routinely estimated in oceanographic studies and has the advantage of capturing a multiscale process in a single scalar value [2] [3]. These turbulence metrics are estimated from Acoustic Doppler Current Profiler (ADCP, volume averaging) data and then tested against estimates from ground-truth Acoustic Doppler Velocimeter (ADV, point measurement) data collected a single height above the seabed, nominally within the rotor sweep of the planned turbine.

The raw alongbeam ADCP data are used to estimate the spatial structure $D(z, r)$ of the turbulence, where z is the vertical location and r is the distance between velocity fluctuations as [4]

$$D(z, r) = \langle (v'(z) - v'(z+r))^2 \rangle. \quad (2)$$

Assuming a cascade of isotropic eddies in the inertial sub-range, $D(z, r)$ has the form $\mathcal{A}r^{2/3} - 2n^2$, where \mathcal{A} is determined for each z and n is the Doppler noise (i.e., the expected standard error) of the observations. The dissipation rate is then given by [5]

$$D(z, r) = \mathcal{C}_v^2 \epsilon^{2/3} r^{2/3} \quad (3)$$

where \mathcal{C}_v^2 is a constant taken to be 2.1.

The ADV data are used to estimate the frequency auto-spectra, $S(f)$, of the turbulence velocities, where f is frequency. Assuming a frozen field of fluctuations advected past the instrument (i.e., Taylor’s hypothesis) and an isotropic cascade of energy through the inertial sub-range (i.e., from eddy scales to Kolmogorov scales), the dissipation rate ϵ is estimated as [6]

$$S(f) = a\epsilon^{2/3} f^{-5/3}, \quad (4)$$

Support for this research provided by the U.S. Department of Energy, Office of Energy Efficiency and Renewable Energy - Wind and Water Power Program.

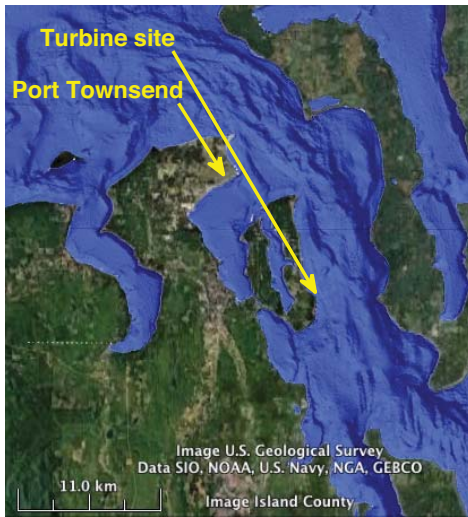


Fig. 1. Location of turbulence observations and proposed site of a tidal turbine demonstration project. [Image from Google Earth, with bathymetry overlay from <http://www.gelib.com/puget-sound-bathymetry.htm>.]

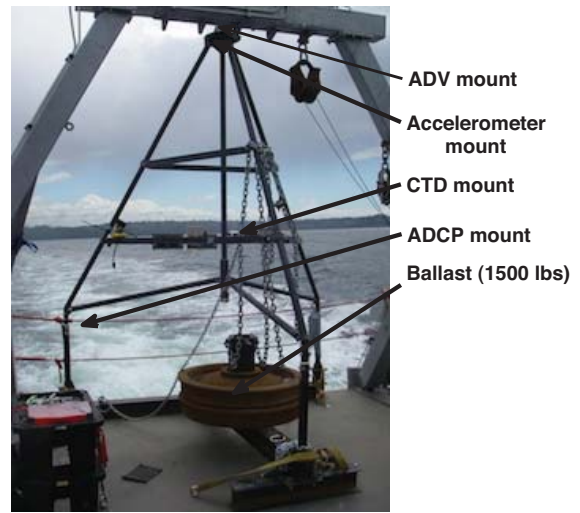


Fig. 2. Tripod, instrument mounts, and ballast prior to deployment from the R/V Jack Robertson (University of Washington Applied Physics Laboratory).

where a is a constant taken to be 0.5. Dissipation rates are multiplied the density of seawater, $\rho = 1024 \text{ Kg/m}^3$, to obtain volumetric dissipation rates in units of W/m^3 .

Finally, ADV data are also used to estimate the coherent TKE, potentially a key parameter controlling vibrational forces on turbines blades.

II. OBSERVATIONS

The site is in 22 m water depth (ref. MLLW) off Nodule Point on Marrowstone Island at $48^\circ 01' 55.154'' \text{ N}$ $122^\circ 39' 40.326'' \text{ W}$. The site and bathymetry are shown in Figure 1 and the instrument tripod is shown in Figure 2. The observations are from a point-measuring Acoustic Doppler Velocimeter (ADV, 32 Hz sampling) mounted 4.6 m above the seabed and a volume-averaging Acoustic Doppler Current Profiler (ADCP, 2 Hz sampling) from 2.1 m above the seabed to the surface at 0.5 m resolution. In addition, conductivity-temperature-depth (CTD) data were recorded to estimate the role of stratification, and accelerometer data are recorded to remove potential contamination of tripod motion in the velocity observations. The 4.6 m height at the apex of the tripod was limited by the A-frame of the R/V Jack Robertson, as well as the ballast required for stability (approx. 1500 lbs, see Figure 2).

A. Acoustic Doppler Velocity Profiler (ADCP) data

The ADCP data collected with a 600 kHz RDI Workhorse Sentinel are recorded in 2 Hz bursts of 128 measurements (64 seconds long) every 30 minutes. This 3% duty cycle was necessary to conserve power and memory over a two-week deployment capturing both spring and neap tides. The raw along-beam data is recorded to avoid the assumption of homogeneity required in the transformation to rectangular coordinates, which is a poor assumption for turbulent fluctuations. The expected standard error, or Doppler noise, of

the raw pings is $n = 0.195 \text{ m/s}$ (horizontal), as given by RDI's PlanADCP software. Ensemble averaging the whole burst reduces this error to 0.017 m/s (i.e., division by the square root of the number of pings). The observed alongbeam velocity fluctuations are up to 0.17 m/s, which is equivalent to 0.56 m/s in the horizontal plane, and are similar between each of the four beams. This suggests isotropy in the turbulent velocity field, in contrast to the clear alignment of beams 3 and 4 along the principal axis of the mean currents (see Figure 3).

Prior to analysis, the ADCP data are quality controlled by removing bins with low acoustic correlation (necessary to compute Doppler velocities), bins at or above the surface, and anomalous spikes. A correlation cutoff of 60 is used, and the first 4 bins below the surface are removed because of acoustic reflections. An example burst of raw data is shown in Figure 3, and the corresponding structure function (Eq. 2) is shown in Figure 4 for the bin equivalent to the ADV height. The similar fits across the four beams suggest isotropy in the turbulent velocity field. A summary of the ADCP data is shown in Figure 5. Consistent with previous observations, the burst mean velocities show a mixed semi-diurnal tide regime, with maximum spring velocity magnitude of almost 2 m/s [7]. The large velocity fluctuations near the surface at the end of the deployment are associated with waves from a storm on 20 May 2010, in which wind speeds exceeded 20 m/s [8].

B. Acoustic Doppler Velocimeter (ADV) data

The ADV data collected with a 6 Mhz Nortek Vector were recorded in 32 Hz bursts of 2048 measurements (64 seconds long) every 10 minutes. This 10% duty cycle was necessary to conserve power and memory over a two-week deployment capturing both spring and neap tides. The sampling scheme was chosen to capture high-frequency fluctuations of velocity within short windows that are quasi-stationary (i.e., stable mean and variance). The expected standard error, or Doppler

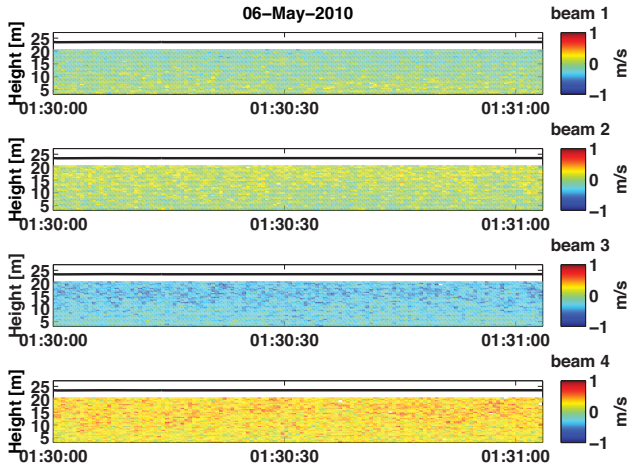


Fig. 3. Example ADCP burst of 128 pings sampled at 2 Hz (beam data by panel). Colorscale indicates velocity magnitude.

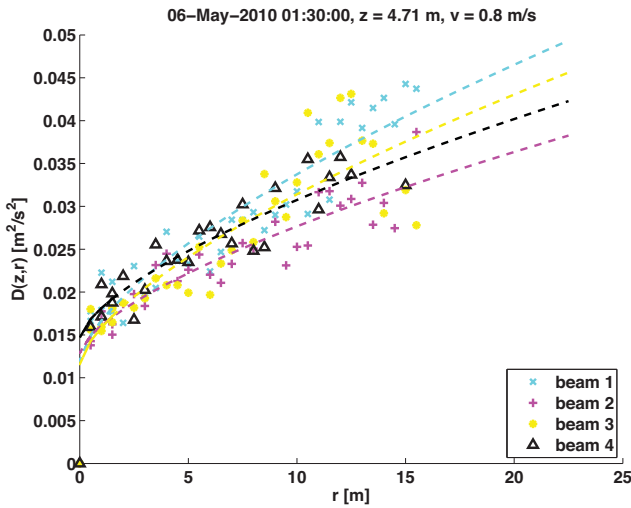


Fig. 4. Example structure function of velocity fluctuations at $z = 4.7$ m above the seabed. Lines and symbols are for different beams of the ADCP. The y-intercept is the result of Doppler noise.

noise, of the raw pings is $n = 0.04$ m/s, according to the 1%-of-range accuracy specification given by Nortek. Ensemble averaging the whole burst reduces this error to 0.0009 m/s (i.e., division by the square root of the number of pings). The velocity fluctuations measured by the ADV are up to 0.18 m/s, for each horizontal component, and 0.1 m/s for the vertical component, respectively.

Prior to analysis, the ADV data are quality controlled by removing points of low acoustic correlation (necessary to compute Doppler shift) and anomalous spikes. The correlation cutoff used is $c = 30 + 40\sqrt{f_s/25}$, where f_s is the sampling rate in Hz [9] [10]. The number of spurious points is typically less than 1% of the total points, and a running mean is used to replace those values. Interpolation across small gaps does not significantly alter the auto-spectra of the velocity records [11]. Figure 6 shows an example of the velocity components,

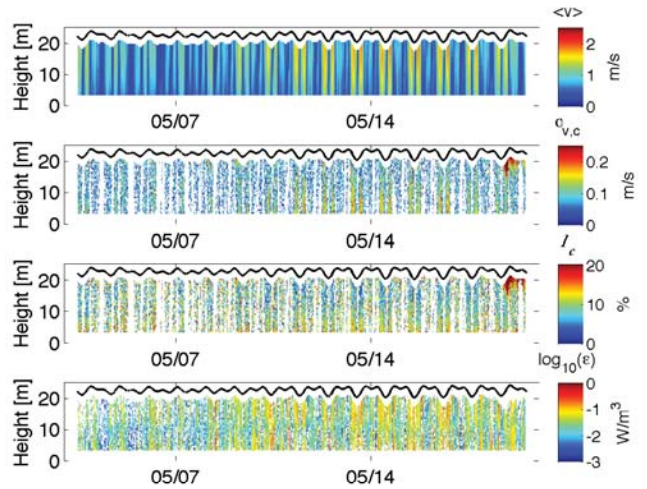


Fig. 5. ADCP estimates of (top to bottom panels): mean velocity magnitude, corrected velocity standard deviations, corrected turbulent intensity, and dissipation rate.

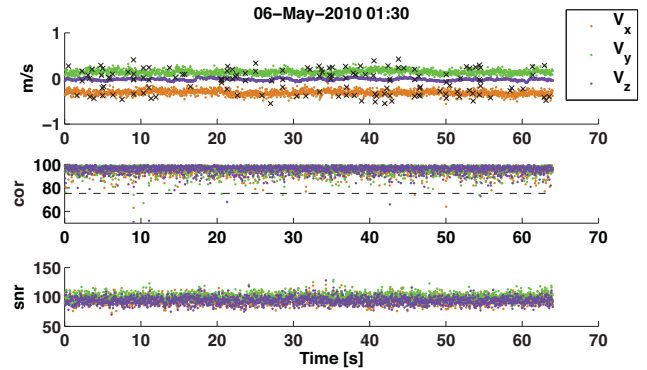


Fig. 6. Example ADV burst of 2048 data points sampled at 32 Hz (top to bottom panels): velocity components, acoustic correlations, and signal-to-noise ratio. Colors indicate components of velocity, and crosses are used to indicate spurious values.

acoustic correlations, and signal strength from a burst.

After quality control, frequency auto-spectra are estimated from each burst using a Fast Fourier Transform (FFT) algorithm on Hamming-tapered windows of on 512-points each, with 50% overlap between windows. The results are ensemble averaged within each burst to obtain final spectra with eight degrees of freedom. Figure 7 shows an example of the spectrum, corresponding to the raw data in Figure 6. The spectra generally show energy decreasing with increasing frequency and exhibit a flat noise-floor at very high frequencies. The noise floor is lower in the vertical velocity auto-spectra, because of bias in the ADV beam alignment (30 deg from vertical, 60 deg from horizontal). The spectra show similar energy levels for each horizontal component, v_x and v_y , suggesting quasi-isotropy of the turbulence. For some bursts, there is suppression of vertical TKE, which an expected consequence of density stratification in a tidal estuary. Note

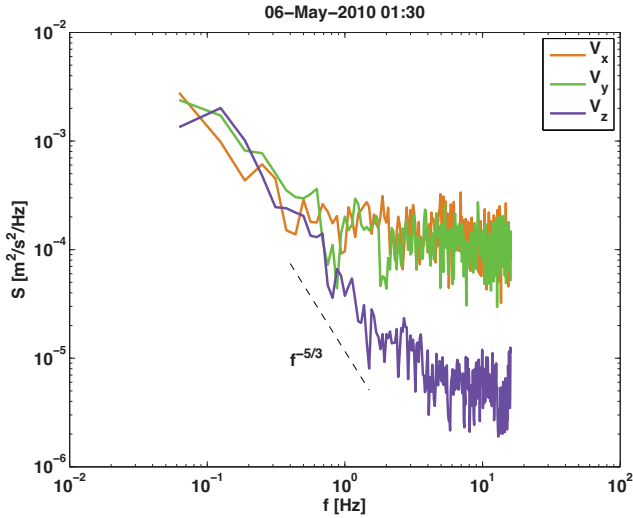


Fig. 7. Example auto-spectra of velocity components, by color. The commonly observed $f^{-5/3}$ shape is shown by the dashed line.

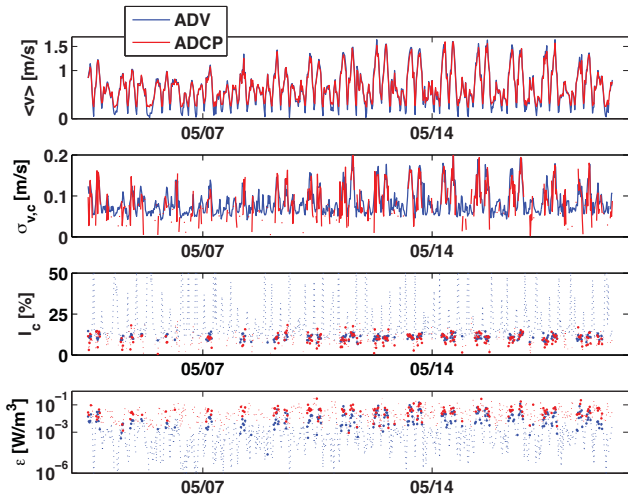


Fig. 8. Time series comparison at $z = 4.6$ m above the seabed of (top to bottom panels): mean velocity magnitude, corrected velocity standard deviation, corrected turbulent intensity, and rate of TKE dissipation. Turbulent intensity and dissipation values are solid or dashed for periods when the burst mean velocity magnitude is above or below 0.8 m/s, respectively.

that the observed noise floor could be used for empirical determination of noise bias in the velocity fluctuations and TKE, instead of using the 1%-of-range specification.

A summary of the ADV data and the corresponding ADCP bin data is shown in Figure 8, and as expected, there is excellent agreement in the mean horizontal current magnitude $\langle v \rangle$. There is also agreement for turbulence metrics (σ_v , I , ϵ , but only after correcting for Doppler noise (§III).

C. Conductivity, Temperature, and Depth (CTD) data

The conductivity, temperature, and depth (CTD) data collected with Sea Bird Electronics SBE 37 were recorded every 30 seconds and are shown in Figure 9. The CTD observations show a typical estuarine exchange flow, in which salinity

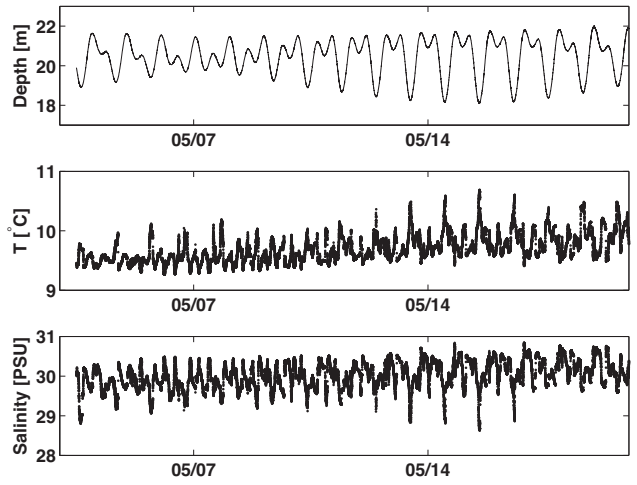


Fig. 9. Time series of (top to bottom panels): depth, temperature, and salinity.

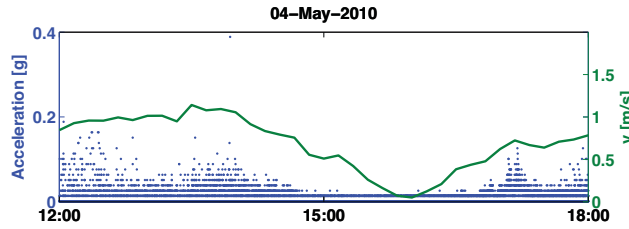


Fig. 10. Tripod horizontal accelerations (blue) and mean currents (green) during the first six hours of the deployment.

decreases on ebb and increases on flood. Temperature is also modulated by the tidal currents, however it is not typically important in setting the densities of estuarine flows [12].

D. Tripod motion

The ADV mount acceleration data collected with a HOBO Pendant-G were recorded at 1 Hz for the first six hours of the deployment. The raw data shown in Figure 10 are correlated with the tidal currents, indicated some motion of the instruments. However, the acceleration spectra are flat (not shown), suggesting no strumming, or tonal, motion was generated that would require correction of velocity auto-spectra. Integrating the accelerations suggests horizontal translations of 2 mm are typical during strong currents.

III. ANALYSIS

Results are summarized in Table I, where estimates of velocity fluctuations, turbulence intensity, and dissipation rate are compared. Comparisons are much improved when slack tides, defined as ADV-height mean currents less than 0.8 m/s, are neglected. This is also the approximate cut-in speed of the tidal turbines under consideration. The remaining non-slack records account for approximately 30% of the data.

A. Turbulent intensity I

Turbulent intensity estimates are shown in Figures 5 & 8, ranging from 5 to 50%. The highest values are all during

TABLE I

SUMMARY OF DOPPLER NOISE, VELOCITY STANDARD DEVIATION, TURBULENT INTENSITY, AND DISSIPATION RATE AT 4.6 M ABOVE THE SEABED. SLACK PERIODS ARE EXCLUDED.

	ADV	ADCP
n [m/s]	0.04	0.195
Average values		
σ_v [m/s]	0.13	0.22
$\sigma_{v,c}$ [m/s]	0.12	0.11
I [%]	12	22
I_c [%]	11	10
ϵ [W/m ³]	0.017	0.043
Maximum values		
σ_v [m/s]	0.22	0.31
$\sigma_{v,c}$ [m/s]	0.21	0.24
I [%]	15	30
I_c [%]	16	18
ϵ [W/m ³]	0.146	0.285

slack periods, because the mean velocities $\langle v \rangle$ in the denominator are small. During strong tides, turbulent intensity is consistently around 10%. Intensities are calculated using full bursts (64 s) as the ensemble timescale indicated by brackets. Important corrections to the raw data, described below, are required to obtain these estimates.

First, direct estimates of turbulent intensity (Eq. 1) are biased high by the standard error, or Doppler noise n , in a burst of raw pings. The measurements of mean velocity magnitude, used to normalize the turbulent intensity, are well-defined because averaging reduces this error. The statistics of velocity fluctuations, however, remain biased by Doppler noise, because this noise contributes additional variance to the signal. The significance of this noise can be seen in Figure 11, in which there is a significant offset between velocity standard deviation from the ADV ($n = 0.04$ m/s) and the equivalent bin of the ADCP ($n = 0.195$ m/s). Indeed, in the limit of perfect laminar flow, Doppler noise would result in an observation of non-zero turbulent intensity. Assuming zero covariance between the Doppler noise and the turbulence, error variance n^2 can be subtracted from the velocity variance $\langle v'^2 \rangle$ to obtain a corrected estimate of velocity standard deviation $\sigma_{v,c} = \sqrt{\sigma_v^2 - n^2} = \sqrt{\langle v'^2 \rangle - n^2}$ and a corrected turbulent intensity

$$I_c = \frac{\sqrt{\langle v'^2 \rangle - n^2}}{\langle v \rangle} = \frac{\sigma_{v,c}}{\langle v \rangle}, \quad (5)$$

where n is dependent on the sampling configuration of the ADCP. Despite the substantial bias in raw σ_v from the ADCP (Figure 11), the corrected velocity standard deviation and corrected turbulence intensity values are in close agreement (Figure 8), demonstrating successful removal of Doppler noise by Eq. 5.

According to the Bienaym theorem for independent variables, the noise correction must be done with the variances (i.e., the squares of the standard deviation σ_v and the standard

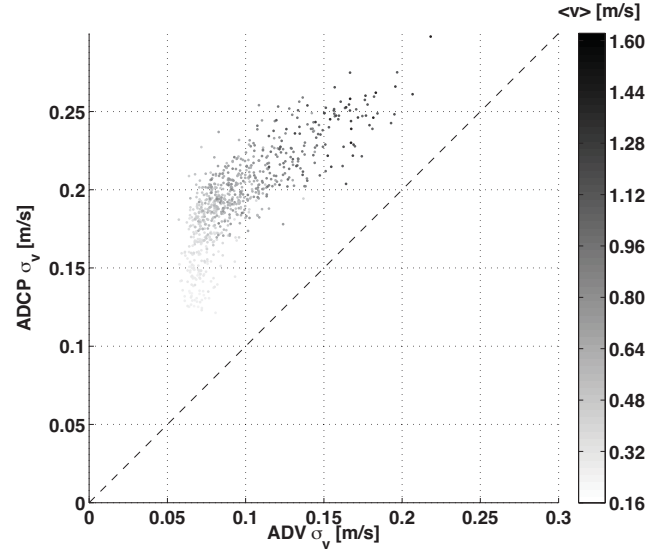


Fig. 11. Observed (uncorrected) velocity standard deviations, by burst, from the ADCP data versus from the ADV data at 4.6 m above the seabed. The grayscale indicates the magnitude of the mean horizontal current.

error n) in order for the correction to be unbiased [13]. This places an appropriate limit on the minimum turbulent intensity that can be measured with a given instrument—the intrinsic noise level of the instrument itself. If the observed velocity variance is less than to the error variance, Eq. 5 will give an imaginary result, indicating the data are not valid for turbulence estimates. For this dataset, that condition applies to only 9% of the non-slack bursts (or 2% of all bursts) and those are excluded from the reported average.

Histograms of the corrected turbulent intensities are shown in Figure 12, neglecting slack periods, where the mean intensity estimated from the ADV is 11% and the mean intensity estimated from the ADCP is 10%. Prior to correcting for the Doppler noise, the intensities were 12% and 22%, respectively. The histograms of corrected turbulent intensity are near-Gaussian, however the ADCP estimates have a much wider distribution. Although the underlying Doppler noise is expected to be Gaussian within a burst, it is not presumed, a priori, that the turbulent intensities would be Gaussian over different stages of the tide.

In addition to Doppler noise, turbulent intensity may be biased by under-sampling the velocity field. As illustrated by the frequency auto-spectra of velocity in Figure 7, TKE varies over a continuous range of timescales, yet the common sampling configuration for ADCPs uses ensemble averages of multiple pings, which span several seconds to a few minutes. Based on the spectral shapes observed here, estimates of turbulent intensity will be increasing biased low for velocity observations at less than 1 Hz. Thus, there is a trade-off between the rapid sampling required to observe σ_v and the elevated noise n of raw pings.

Finally, for ADCP measurements, the coordinate transformation necessary to determine horizontal velocities from beam

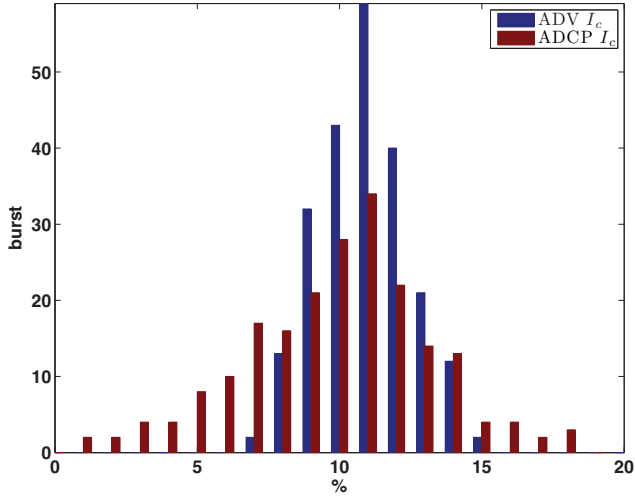


Fig. 12. Histograms of corrected turbulent intensity, by burst, from the ADV data and from the ADCP data at 4.6 m above the seabed.

data may bias estimates of turbulent intensity. The coordinate transform assumes homogeneity across the different beams, which diverge with range. While this may be acceptable for mean currents, the true turbulent fluctuations along each beam will be averaged into a single horizontal value and may be reduced. Instead, the alongbeam fluctuations can be retained and projected individually to the horizontal plane (division by $\cos(70^\circ)$), while still using the transformed horizontal mean for normalization. This assumes isotropy of the turbulent fluctuations and homogeneity of the mean currents, but does not assume homogeneity of the turbulent fluctuations from one beam to another. For this dataset, the results are similar between the alongbeam and transformed approaches, suggesting homogeneity and isotropy are both valid, but this may not be the case for other sites.

B. Dissipation rate ϵ

Dissipation rate estimates are shown in Figures 5 & 8. The dissipation rate is generally minimal during slack periods ($\epsilon \approx 10^{-6} \text{ W/m}^3$) and maximal during periods of strong mean flow ($\epsilon \approx 10^{-1} \text{ W/m}^3$). The maximum dissipation rate observed for the whole deployment is $3 \times 10^{-1} \text{ W/m}^3$. These values are well within the oceanographic range of 10^{-8} W/m^3 in the abyssal ocean and 10^1 W/m^3 in the surfzone. Compared with turbulent intensity, the dissipation rate has more dynamic range and more consistent trends from slack to strong flow periods. However, the dissipation rate is more sensitive to Doppler noise and agreement between the ADV and ADCP is worse. Figure 13 shows weak agreement for strong flows ($\langle v \rangle > 1.2 \text{ m/s}$) and no agreement at lower velocities. This likely because the velocity fluctuations are too small to stand out from the Doppler noise of the ADCP.

C. Depth dependence

It is well-known that tidal currents increase with distance from the bottom, and this is an important consideration for

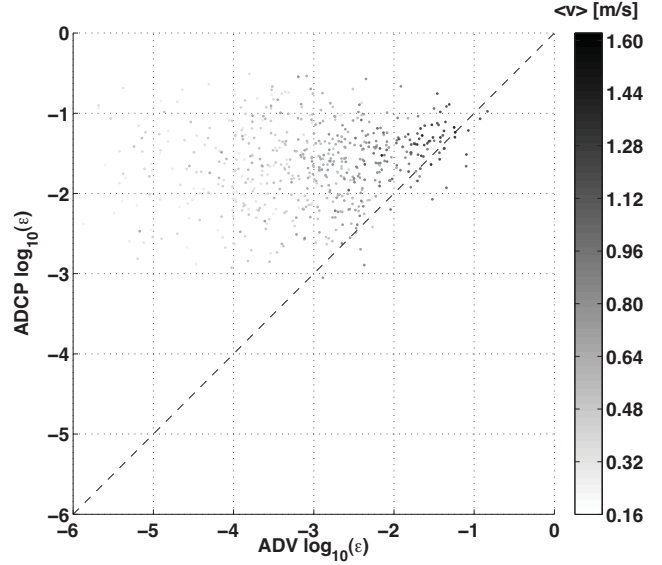


Fig. 13. Dissipation rate, by burst, from the ADV data versus from the ADCP data at 4.6 m above the seabed. The grayscale indicates the magnitude of the mean horizontal current.

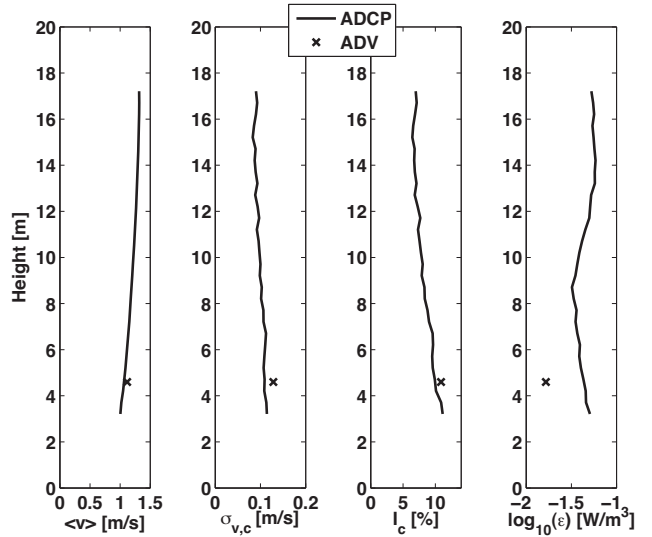


Fig. 14. Average vertical dependence of (left to right panels): mean velocity magnitude, corrected velocity standard deviation, corrected turbulent intensity, and dissipation rate. Vertical axis is height above the seabed.

siting tidal power turbines [14], since kinetic power density scales with v^3 . Figure 14 shows the mean vertical dependence of turbulence metrics, which generally decrease with height above the seabed. Although all metrics indicate less turbulence with height, the difference appears insufficient to drive foundation design (compared with increased power density).

D. Coherent TKE

Coherent turbulence can be characterized by coherent turbulent kinetic energy E_{coh} which is defined as

$$E_{coh} = \frac{1}{2} \langle [v'_x v'_z]^2 + [v'_x v'_y]^2 + [v'_y v'_z]^2 \rangle, \quad (6)$$

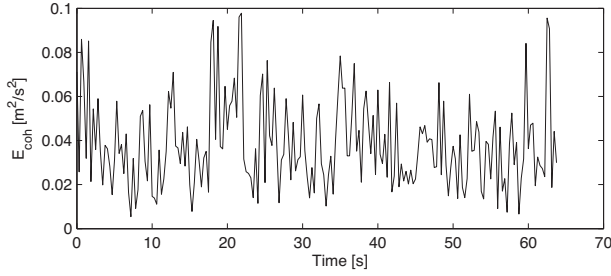


Fig. 15. E_{coh} for ADV survey performed on 06 May 2010 at 01:30 hrs.

where v'_x , v'_y , and v'_z are the velocity fluctuations in the x , y and z directions, respectively. The potential importance of coherent turbulence on the operation of hydro-kinetic devices is illustrated by a study done by Kelley et. al. [15] on wind turbine blades, which suggests that blade fatigue damages occur during night time from coherent turbulence in the atmospheric boundary layer. Figure 15 shows the E_{coh} for the ADV survey performed on 06 May 2010 at 01:30 hrs. From this figure, the impact of E_{coh} on the hydro-kinetic devices is not obvious. Wavelet analysis [15] is therefore used to understand the time-frequency behavior of E_{coh} and its impact on hydro-kinetic devices. Following Kelley and Osgood, a continuous wavelet transform function, with a Morlet wavelet as the mother function, is used. The time-frequency spectrum analysis for E_{coh} is shown in Figure 16 (red represents the highest energy and blue represents lowest energy). As shown in the figure, E_{coh} has energy in both lower as well as higher frequencies; at higher frequencies, the structures are difficult to observe due to non-linear nature of the frequency scale. This approach is similar to that used by Kelley et. al. [16]. In their study, a 1:1 correspondence was observed between the spectral frequencies of coherent turbulence (E_{coh}) and vibratory response of the turbine blades. They described this phenomenon as “resonant coupling”, and suggested it to be the reason for blade fatigue damage in wind turbines. Hydro-kinetic devices may show behavior similar to that of wind turbines; hence the approaches used to interpret the results obtained from experiments pertaining to wind turbines can be extrapolated to experiments performed on hydro-kinetic devices as well, albeit with caution. Based on the time-frequency behavior of E_{coh} obtained in this study, hydro-kinetic devices may be expected to exhibit similar response at higher frequencies due to the presence of energies at these frequencies in the E_{coh} . However, further detailed study and thorough analysis needs to be performed in order to conclusively demonstrate and understand the structural response of hydro-kinetic devices in various inflow conditions.

IV. CONCLUSIONS & FUTURE WORK

Using newly collected data from a tidal power site in Puget Sound, WA, metrics for turbulence quantification are assessed and compared. A large tripod deployment was successful in getting high-frequency observations of fluid velocity

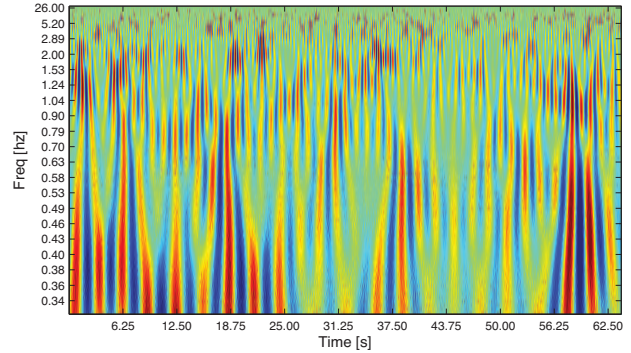


Fig. 16. Time-frequency spectral decomposition of E_{coh} for ADV survey performed on 06 May 2010 at 01:30 hrs.

fluctuations within the planned rotor sweep of a turbine. The fluctuations are shown to be largely isotropic, despite strong bi-directionality in the mean tidal currents.

A key finding is the necessity of removing Doppler noise when estimating second order statistics of velocity observations. For velocity standard deviations and subsequent turbulence intensities, the variance contribution by Doppler noise can be subtracted directly from the raw velocity variance. After removal of Doppler noise, mean turbulence intensities from this dataset are 10% during periods in which turbines would operate. For the dissipation rate of turbulent kinetic energy (TKE), the noise is removed as an offset during spectral (Eq. 4) or structure (Eq. 3) fitting. The dissipation rate is more variable and only shows a loose agreement between the ADV and ADCP under conditions of strong currents.

Future work will continue investigation of coherent TKE, as well as evaluation the full TKE budget,

$$\frac{D}{Dt}(TKE) + \nabla \cdot \mathcal{T} = \mathcal{P} - \epsilon, \quad (7)$$

where $\frac{D}{Dt}$ is the material derivative (of the mean flow), \mathcal{T} is the turbulent transport, \mathcal{P} is production (via shear and buoyancy) and ϵ is dissipation (loss to heat and sound). Understanding the full TKE budget may improve understanding of the residual currents unexplained by harmonic analyses and may improve predictions of turbulent feedback mechanisms during turbine operation.

ACKNOWLEDGEMENTS

Thanks to Joe Talbert for design and assembly of the instrument tripod, as well as participation in deployment and recovery. Thanks to Sequoia Scientific for the original upper section of the tripod. Thanks to Andy Jessup for loan of the SBE 37 CTD. Pacific Northwest National Laboratory (PNNL) in Richland, Washington, is operated by Battelle Memorial Institute for the U.S. Department of Energy.

REFERENCES

- [1] S. Thorpe, *An introduction to Ocean Turbulence*. Cambridge Univ. Press, 2007.
- [2] Y. Lu and R. G. Lueck, “Using a broadband adcp in a tidal channel. part ii: Turbulence,” *J. Atmos. Ocean. Tech.*, vol. 16, pp. 1568–1579, 1999.

- [3] T. P. Rippeth, J. H. Simpson, E. Williams, and M. E. Inall, "Measurements of the rates of production and dissipation of turbulent kinetic energy in an energetic tidal flow: Red warf bay revisited." *J. Phys. Oceanogr.*, vol. 33, pp. 1889–1901, 2003.
- [4] P. Wiles, T. P. Rippeth, J. Simpson, and P. Hendricks, "A novel technique for measuring the rate of turbulent dissipation in the marine environment." *Geophys. Res. Let.*, vol. 33, p. L21608, 2006.
- [5] A. E. Gargett, "Velcro measurement of turbulence kinetic energy dissipation rate epsilon," *J. Atmos. Ocean. Tech.*, vol. 16, no. 12, pp. 1973–1993, 1999.
- [6] J. L. Lumley and E. Terray, "Kinematics of turbulence convected by a random wave field," *J. Phys. Oceanogr.*, vol. 13, pp. 2000–2007, 1983.
- [7] S. Gooch, J. Thomson, B. Polagye, and D. Meggitt, "Site characterization for tidal power," in *MTS/IEEE Oceans 2009*, Biloxi, MI, Oct 26-29 2009.
- [8] NDBC Station SISW1 - Smith Island, WA.
- [9] S. Elgar, B. Raubenheimer, and R. T. Guza, "Current meter performance in the surfzone," *J. Atmos. Ocean. Tech.*, vol. 18, pp. 1735–1746, 2001.
- [10] —, "Quality control of acoustic doppler velocimeter data in the surfzone," *Measur. Sci. Tech.*, vol. 16, pp. 1889–1893, 2005.
- [11] F. Feddersen, "Quality controlling surfzone acoustic doppler velocimeter observations to estimate the turbulent dissipation rate," *J. Atmos. Ocean. Tech.*, vol. submitted, 2010.
- [12] P. MacCready and W. R. Geyer, "Advances in estuarine physics," *Annual Review of Marine Science*, vol. 2, pp. 35–38, 2010. [Online]. Available: 10.1146/annurev-marine-120308-081015
- [13] M. Loeve, *Probability Theory*, 4th ed., ser. Graduate Texts in Mathematics. Springer-Verlag, 1977.
- [14] M. Kawase, P. Beda, and B. C. Fabien, "Finding and optimal placement depth for a tidal in-stream energy conversion device in an energetic, baroclinic tidal channel," *J. Power and Energy*, submitted.
- [15] N. D. Kelley and R. M. Osgood, "Using time-frequency and wavelet analysis to assess turbulence/rotor interactions," in *19th American Society of Mechanical Engineers Wind Energy Symposium*, 2000.
- [16] N. D. Kelley, J. Jonkman, N. Scott, J. Bialasiewicz, and L. S. Redmond, "Impact of coherent turbulence on wind turbine aeroelastic response and its simulation," NREL, Tech. Rep. CP-500-38074, 2005.